Biointerface Research in Applied Chemistry
Open-Access Journal (ISSN: 2069-5837)

Article
Volume 16, Issue 2, 2026, 43
https://doi.org/10.33263/BRIAC162.043

Influence of Mefenamic Acid on the Behavior of Stainless Steel 316 in 6% H_2O_2 and Normal Saline: An Electrochemical and Computational Study

Msenhemba Moses Mchihi [1,*], Elizabeth Ayomide Koleoso [1], Nnenna Winifred Odozi [2,*]

[1] Department of Chemical Science, School of Science, Yaba College of Technology, Lagos; msenhemba.mchihi@yabatech.edu.ng (M.M.M.); elizabethkoleoso73@gmail.com (E.A.K.);
[2] Department of Chemistry, Faculty of Science, University of Ibadan, Ibadan, Nigeria; nw.odozi@ui.edu.ng (N.W.O);
* Correspondence: msenhemba.mchihi@yabatech.edu.ng (M.M.M.); nw.odozi@ui.edu.ng (N.W.O);

Received: 7.12.2025; Accepted: 20.02.2026; Published: 15.04.2026

Abstract: The study investigated the effects of mefenamic acid (MA) on the behavior of stainless steel 316 when immersed in three environments: a 2:1 mixture of hydrogen peroxide and normal saline (2H:1S), normal saline (S), and a 50:50 mixture of hydrogen peroxide and normal saline (SH). The corrosion potential exhibited a minor positive shift of less than 85 mV, indicating that the inhibitor operates as a mixed-type inhibitor, effectively reducing both anodic and cathodic reactions. The corrosion current density (I_{corr}) decreased significantly from 1775.7 µA/cm² to 123 µA/cm² in the 2H:1S, resulting in an inhibition efficiency (IE) of 93.1%. The I_{corr} values in S and SH solutions fell to 311 µA/cm² and 262 µA/cm², respectively, corresponding to inhibition efficiencies of 82.5% and 85.2%. The findings from electrochemical impedance spectroscopy indicated that in the 2H:1S, the charge transfer resistance (R_{ct}) increased from 708.40 Ω·cm² in the absence of MA to 11070 Ω·cm² for the inhibited system, demonstrating an IE of 93.6%. In the S and SH solutions, R_{ct} values exhibited significant elevations, ascending to 4100 Ω·cm² and 4500 Ω·cm², respectively. Computational analysis revealed that MA is likely to show greater electronic stabilization and heightened electrophilic character in water, resulting in enhanced reactivity.

Keywords: corrosion; density functional theory; stainless steel; corrosion inhibitor.

1. Introduction

Medical-grade stainless steel, particularly the 304 and 316/L variants, is employed in biomedical applications owing to its exceptional durability and biocompatibility [1]. Biomaterials have numerous applications in the medical field [2], including, but not limited to, surgical instruments, vascular devices, tissue replacement and augmentation, controlled drug delivery systems, and scaffolds for tissue engineering [3]. The stainless steel grades 304 and 316/L are predominantly austenitic and are commonly used for surgical instruments, implants, and various medical devices due to their ability to withstand effective sterilization. Among the austenitic grades, 304 and 316/L are widely recognized, with the key distinction being the inclusion of molybdenum in 316, which notably enhances its corrosion resistance [4], particularly in chloride-rich environments [5-7]. The 316L variant, characterized by its low carbon content, exhibits reduced susceptibility to corrosion when welded, rendering it

particularly suitable for use in thicker components. While stainless steels are recognized for their relative stability, they are nonetheless susceptible to chemical corrosion, which can lead to the leaching of hazardous metal ions [8]. This gradual deterioration may also adversely affect the material's inherent physico-mechanical properties over time [5]. A variety of metals and alloys are prone to corrosion when exposed to strong acids, elevated chloride concentrations, hydrogen peroxide [9,10], and other corrosive agents. For example, Xu *et al*. [11] posited that chloride ions (Cl^-) in bodily fluids can damage the protective layer on medical-grade stainless steel alloys, leading to pitting corrosion. Consequently, it can be concluded that despite ongoing research efforts aimed at improving the corrosion resistance of stainless steel, it remains susceptible to corrosion due to the intricate and dynamic physiological conditions present within the human body, as well as the potential exposure to a variety of substances (both within and outside of the body) that possess intricate chemical compositions. [11-13].

H_2O_2 functions as an antiseptic and disinfectant, commonly used for the treatment of minor cuts and abrasions. H_2O_2 is typically applied topically to assist in the removal of impurities, pus, and blood from superficial wounds. Saline solution is also used for wound cleansing, nasal passage irrigation, and as an intravenous (IV) fluid, supporting patient hydration by helping maintain electrolyte balance and addressing fluid loss. H_2O_2, combined with normal saline in equal parts, is frequently used to irrigate traumatic wounds during a range of plastic and reconstructive surgical procedures. These include, but are not limited to, hand surgery, breast reduction, abdominoplasty, lymph node dissections, as well as acute and chronic wound debridement [14]. The interaction of H_2O_2, saline solution, and stainless steel in medical contexts may result in corrosion. This concern is particularly significant given that stainless steel implants are perpetually subjected to physiological fluids, which are a mixture of saline and other constituents. The use of H_2O_2 for disinfection or as a byproduct of inflammatory responses can lead to direct reactions with the steel's surface, as documented in several studies addressing the deterioration of steel by peroxides. Interactions may also arise between saline solutions, H_2O_2, or their combinations when used on stainless steel containers or surgical instruments utilized in medical facilities. A review of the existing literature has highlighted a significant lack of information regarding the electrochemical properties of stainless steel 316 when exposed to saline solution, a 2:1 mixture of hydrogen peroxide and saline, and a 50:50 blend of saline solution and hydrogen peroxide. Likewise, there is limited documentation concerning the effects of potential corrosion inhibitor candidates on the electrochemical behavior of stainless steel 316 in these specific environments.

Researchers have conducted numerous investigations into the degradation of stainless steel in various environments [19]. Krasnodebska-Ostrega *et al*. [20] examined the corrosion process of stainless steel grade 316L in natural brine, focusing on the release of chromium and iron. Their results indicated that electrochemically accelerated corrosion led to an uneven release of the steel's components, revealing that chromium is less readily released into the solution compared to iron. Over a short period of 1 week, the interaction between brine and stainless steel resulted in negligible amounts of iron and chromium being released, which is not significant for therapeutic applications [20]. Similarly, Gudic *et al*. [21] investigated the anodic and spontaneous corrosion behaviors of various stainless steel types (AISI 304L, AISI 316L, and 2205 duplex stainless steel) in phosphate-buffered saline (PBS) at a physiological pH of 7.4 and a temperature of 37°C. Light microscopy and SEM/EDS analyses conducted following pitting and spontaneous corrosion revealed surface degradation on AISI 304L and AISI 316L, whereas the 2205 duplex stainless steel (DSS) exhibited minimal corrosion-related

damage. The researchers concluded that the susceptibility of the assessed steel alloys to localized corrosion decreases in the following order: AISI 304L < AISI 316L < 2205 DSS [21]. An investigation into the pitting corrosion resistance of 304 stainless steel was performed in environments of NaCl and H_2SO_4 [22]. The results indicated that the weight loss and corrosion rate of 304 stainless steel were greater in H_2SO_4 than in NaCl, and the polarization curves illustrated that higher concentrations of NaCl corresponded to a more elevated potential at which pitting initiates. The surface morphologies of corroded 304 stainless steel across various concentrations of H_2SO_4 demonstrated considerably more pitting corrosion and significant damage to the passive layer compared to those in NaCl solution [22].

Given the recognized toxicity of traditional inorganic inhibitors, extensive research has focused on evaluating the effectiveness of environmentally benign compounds as corrosion inhibitors. A significant portion of these studies has concentrated on exploring the inhibitory characteristics of a diverse range of biocompatible organic compounds that include heteroatoms, specifically nitrogen, oxygen, sulfur, and phosphorus, as well as multiple bonds [23]. These compounds have the potential to serve as efficient barriers, offering robust protection by adsorbing onto metallic surfaces and obstructing one or more corrosion reactions at the interface between the metal and the solution [23-25].

Mefenamic acid, which is classified as a nonsteroidal anti-inflammatory drug (NSAID) for the management of mild to moderate pain, is composed of heteroatoms that feature lone pairs of electrons. These lone pairs, combined with the electron-rich π system present in the aromatic rings, can interact with the vacant d-orbitals of metal atoms, thereby establishing a protective barrier that prevents corrosive agents from reaching the metal. Although numerous NSAIDs can mitigate corrosion, their efficacy often depends on the molecular configuration that facilitates the formation of a stable protective film. The unique molecular arrangement of mefenamic acid, characterized by the presence of two methyl groups and a diphenylamine backbone, may enable it to generate a more dense or hydrophobic protective layer in comparison to other NSAIDs. The aim of this study is to evaluate the impact of mefenamic acid on the electrochemical properties of stainless steel 316 immersed in various solutions, including a 1:2 mixture of hydrogen peroxide and normal saline (2H:1S), normal saline (S), and a 50:50 combination of saline and hydrogen peroxide (SH).

2. Materials and Methods

2.1. Electrochemical analysis.

Electrochemical assessments were performed in distinct formulations, designated as 2H:1S, S, and SH, which serve as corrosive electrolytes. The open circuit potential (OCP) was monitored over a period of 1800 seconds (30 minutes) to facilitate the dissipation of the charging current and to ensure system stability. This procedure is essential for allowing the metal to dissolve at its equilibrium or free potential (E_{corr}), which is reached under stable OCP conditions. Subsequent electrochemical experiments were conducted while maintaining these OCP conditions. The electrochemical evaluations utilized a cell assembly composed of three electrodes, including a 1 cm^2 exposed stainless steel surface functioning as the working electrode (WE) and a silver/silver chloride (Ag/AgCl) reference electrode (RE). In this study, all electrochemical potentials reported were referenced against Ag/AgCl, with a platinum wire serving as the counter electrode (CE). The electrochemical impedance spectroscopy (EIS) was performed with a perturbation amplitude of 10 mV across a frequency spectrum ranging from

100 kHz to 10 mHz. The investigation of potentiodynamic polarization was executed within a potential range relative to the open-circuit potential (OCP) at a scan rate of 0.2 mV s^{-1}. Measurements were performed twice. Subsequent analysis of the data was conducted using the Zsimpwin 3.2 software for EIS, incorporating a fitted equivalent circuit tailored to the specific metal/electrolyte system, while EC-lab was employed for the analysis of the potentiodynamic polarization data. R_{ct} values were utilized to compute the inhibition efficiency, according to equation 1 [26], where R_{ct} indicates the resistance to charge transfer in the presence of MA, while R^{o}_{ct} represents the charge transfer resistance in the absence of MA. Similarly, the I_{corr} values obtained from PDP analysis were employed to calculate IE using equation 2, where I^{o}_{corr} = corrosion current density in the absence of MA, while I_{corr} = corrosion current density in the presence of MA [27].

$$IE = \frac{Rct - R°ct}{Rct} X\ 100 \quad (1)$$

$$IE = \frac{I°corr - Icorr}{I°corr} X\ 100 \quad (2)$$

2.2. Theoretical studies.

Theoretical examinations were carried out using the Density Functional Theory (DFT) approach at the hybrid functional level, specifically the Becke 3 Lee Yang Par (B3LYP), utilizing a 6-31G(D) basis set and facilitated by the Spartan 14 (version 1.2.0) program, aimed at optimizing mefenamic acid in the gas phase. In addition, computations were carried out utilizing Gaussian '09 and GaussView 6.0, adhering to the B3LYP/6-311++G(d,p) theoretical framework in vacuum and water. This was done to reveal molecular properties that describe the global reactivity of the inhibitor species, including the highest occupied molecular orbital (HOMO), lowest unoccupied molecular orbital (LUMO), the energies of LUMO (E_{LUMO}) and HOMO (E_{HOMO}), the energy gap (ΔE), electronegativity (χ), softness (σ), global hardness (η), the fraction of electrons transferred (ΔN), and the electrophilicity index (ω). The E_{HOMO} and E_{LUMO} relate to the ionization potential (I) and electron affinity (A) as expressed in equations (3) and (4), respectively [28]. The parameters ΔE, χ, η, σ, ω, and ΔN were computed according to equations (5) to (10), respectively [28,29].

$$I = - E_{HOMO} \quad (3)$$

$$A = - E_{LUMO} \quad (4)$$

$$\Delta E = E_{LUMO} - E_{HOMO} \quad (5)$$

$$\chi = \frac{I + A}{2} \quad (6)$$

$$\eta = \frac{I - A}{2} \quad (7)$$

$$\sigma = \frac{1}{\eta} \quad (8)$$

$$\omega = \chi^2/2\eta \quad (9)$$

The degree of electron transfer from the inhibitor to the metal can be approximated using equation 10, assuming χFe = 7.0 eV and η_{Fe} = 0:

$$\Delta N = (\chi_{Fe} - \chi_{inh}) / [2(\eta_{Fe} + \eta_{inh})] \quad (10)$$

3. Results and Discussion

3.1. Open circuit potential (OCP) analysis.

The analysis of open circuit potential (OCP), as illustrated in Figures 1a, 1b, and 1c, demonstrates the time-dependent variations of potential for stainless steel samples subjected to both uninhibited (blank) and in the presence of 0.5 g/L of mefenamic acid (MA) across three distinct corrosive environments (2H:1S, S, and SH solutions). In all instances, a shift in OCP was observed in the presence of mefenamic acid. In 2H:1S and SH, the OCP of the inhibited system clearly exhibited a shift toward more positive (noble) values in comparison to the blank sample. This phenomenon indicates that the inhibitor molecules influenced the electrochemical behavior of SS-316 in the studied media [15]. This could be due to the effective adsorption of the inhibitor molecules onto the metal surface, thereby forming a protective barrier film that reduces anodic iron dissolution and inhibits cathodic hydrogen evolution. According to El Boraei *et al*. [3], a substantial movement of the OCP in the direction of positive values could indicate the ability of the alloy to produce a passive layer on its surface that reduces the rate of corrosion.

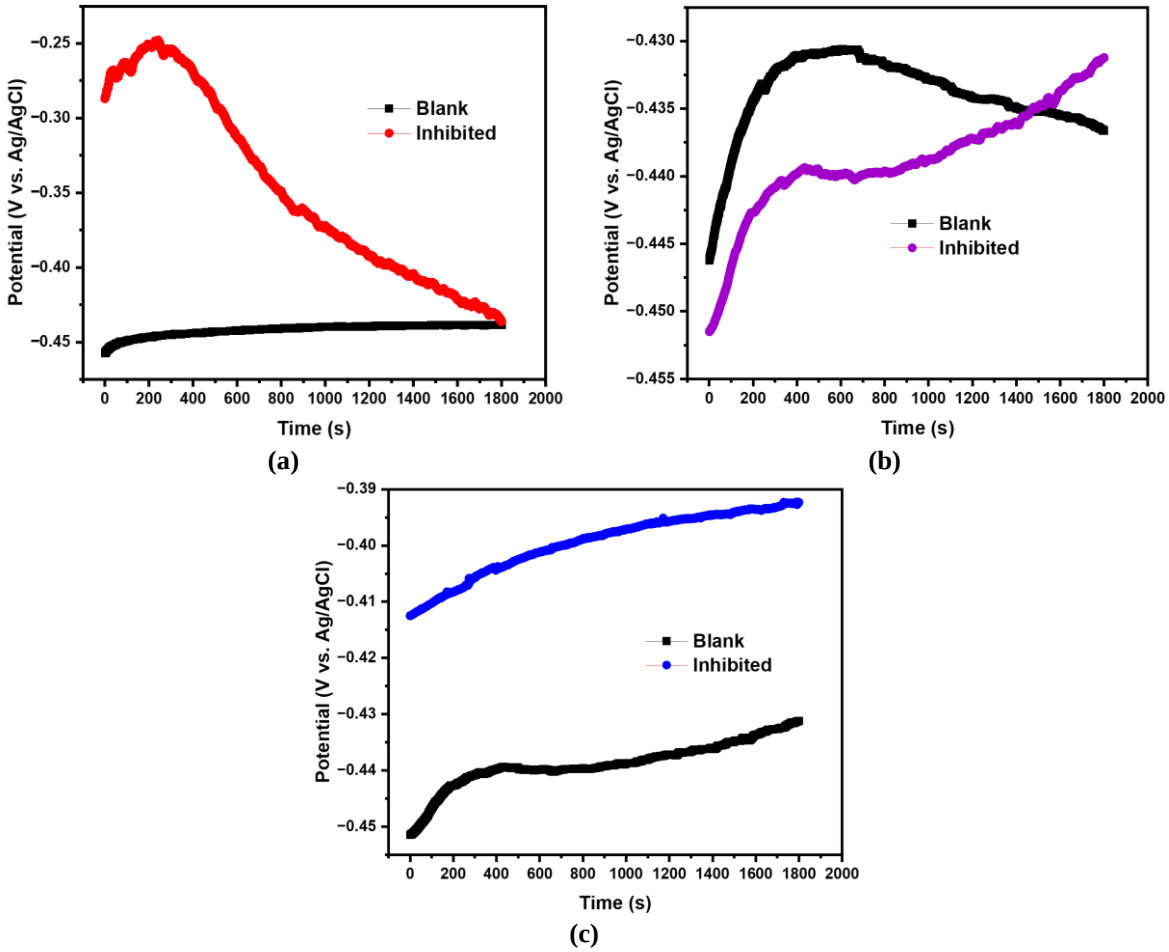

Figure 1. OCP plots of stainless steel for blank uninhibited system in comparison with the inhibited, tested in **(a)** 2H:1S environment; **(b)** S environment; **(c)** SH environment.

3.2. Analysis of potentiodynamic polarization (PDP).

The potentiodynamic polarization (PDP) curves, illustrated in Figures 2a, 2b, and 2c, along with the data presented in Table 1, indicate marked distinctions between the uninhibited and inhibited systems. The corrosion potential (E_{corr}) showed a slight positive shift of less than

85 mV [30]. This minor shift implies that the inhibitor functions as a mixed-type inhibitor, effectively diminishing both anodic and cathodic reactions [31]. The observed reductions in both anodic (βa) and cathodic (βc) Tafel slopes for the inhibited systems indicate that mefenamic acid influenced the kinetics of both the anodic and cathodic reactions [12]. This suggests that the inhibitor molecules retard both metal oxidation and hydrogen ion reduction processes. In the case of the 2H:1S solution, an inhibition efficiency (IE) of 93.1% was achieved. Likewise, in the S and SH solutions, the inhibition efficiencies of 82.5% and 85.2% were obtained, respectively. That is, in the case of the 2H:1S solution, I_{corr} decreased from 1776 µA/cm² to 123 µA/cm², achieving an inhibition efficiency (IE) of 93.1% [32]. Likewise, in the S and SH solutions, I_{corr} values diminished to 311 µA/cm² and 262 µA/cm², correlating to efficiencies of 82.5% and 85.2%, respectively. This illustrates the potent protective properties of the inhibitor, which may result from the formation of an adherent, stable film on the surface of stainless steel, effectively preventing aggressive species from contacting the metal [33-35].

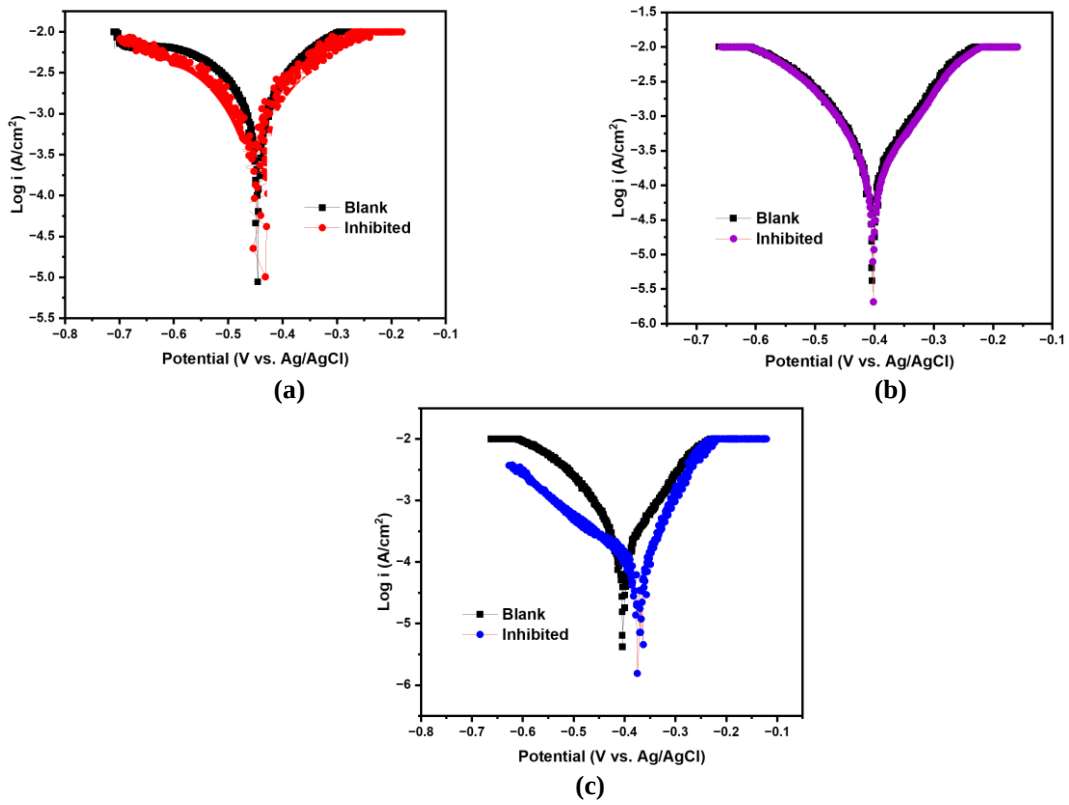

Figure 2. PDP plots of stainless steel for blank uninhibited system in comparison with the inhibited, tested in **(a)** 2H:1S medium; **(b)** S medium; **(c)** SH medium.

Table 1. Potentiodynamic polarization parameters relating to stainless steel for an uninhibited system in comparison with the inhibited, tested in diverse environments.

Medium	System	E_{corr} / mV/Ag/AgCl	I_{corr} / µAcm^{-2}	βa / mVdec^{-1}	βc / mVdec^{-1}	θ	IE /%
2H:1S	Blank	-425	1775.7	87	109	-	-
	inhibited	-420	123	51	78	0.931	93.1
Saline	Blank	-401	1776.4	71	87	-	-
	inhibited	-400	311	67	64	0.825	82.5
SH	Blank	-401	1775.5	72	78	-	-
	inhibited	-399	262	68	65	0.852	85.2

3.3. Electrochemical impedance spectroscopy (EIS) analysis.

The Nyquist (Figures 3a, 3b, 3c) and Bode plots (Figures 4, 5, 6), along with the related impedance data (Table 2), provide further insight into the corrosion inhibition mechanism. The noticeable similarities in the configuration of the impedance semicircle for SS-316 observed in

both inhibited and uninhibited systems indicate that mefenamic acid did not modify the corrosion mechanism of SS-316 in 2H:1S, S, and SH environments. The Nyquist plots across all systems exhibit a singular semicircular loop, signifying that charge transfer predominantly governs the corrosion process [35]. The observed deviations from an impeccable circular outline could be ascribed to interfacial impedance frequency dispersion [35,36]. The electrical equivalent circuit utilized for the analysis of EIS data is depicted in Figure 7. In this representation, R_s denotes the solution resistance, R_{ct} represents the charge transfer resistance, and CPE refers to the constant phase element [33]. The findings indicated the presence of two non-ideal capacitances, labeled as CPE1 and CPE2, attributed to surface heterogeneity between the SS-316 substrate and the adjacent film. An increase in the CPE magnitude (Q) typically suggests water absorption or infiltration, which subsequently results in enhanced corrosion effects on the metal [33]. In all instances, the deviation parameter, n, is close to unity, indicating the pseudocapacitive behavior of the electrode/solution interface. The inhibited systems present significantly larger semicircle diameters, which correlate with enhanced charge transfer resistance (Rct) values [37,38], resulting in decreased corrosion rates. For example, in the 2H:1S solution, R_{ct} rose from 708.4 Ω·cm² in the absence of MA to 11070 Ω·cm² for the inhibited sample, reflecting a 93.6% efficiency in inhibition. In a similar fashion, the R_{ct} values for the S and SH solutions exhibited a significant increase, rising from 707.9 Ω·cm² to 4100 Ω·cm² and 708.2 to 4500 Ω·cm², respectively, which corresponds to inhibition efficiencies of 82.7% and 84.3%. The upsurge of R_{ct} in the presence of an inhibitor could be due to adsorption of the inhibitor molecules on the stainless steel surface [23,37].

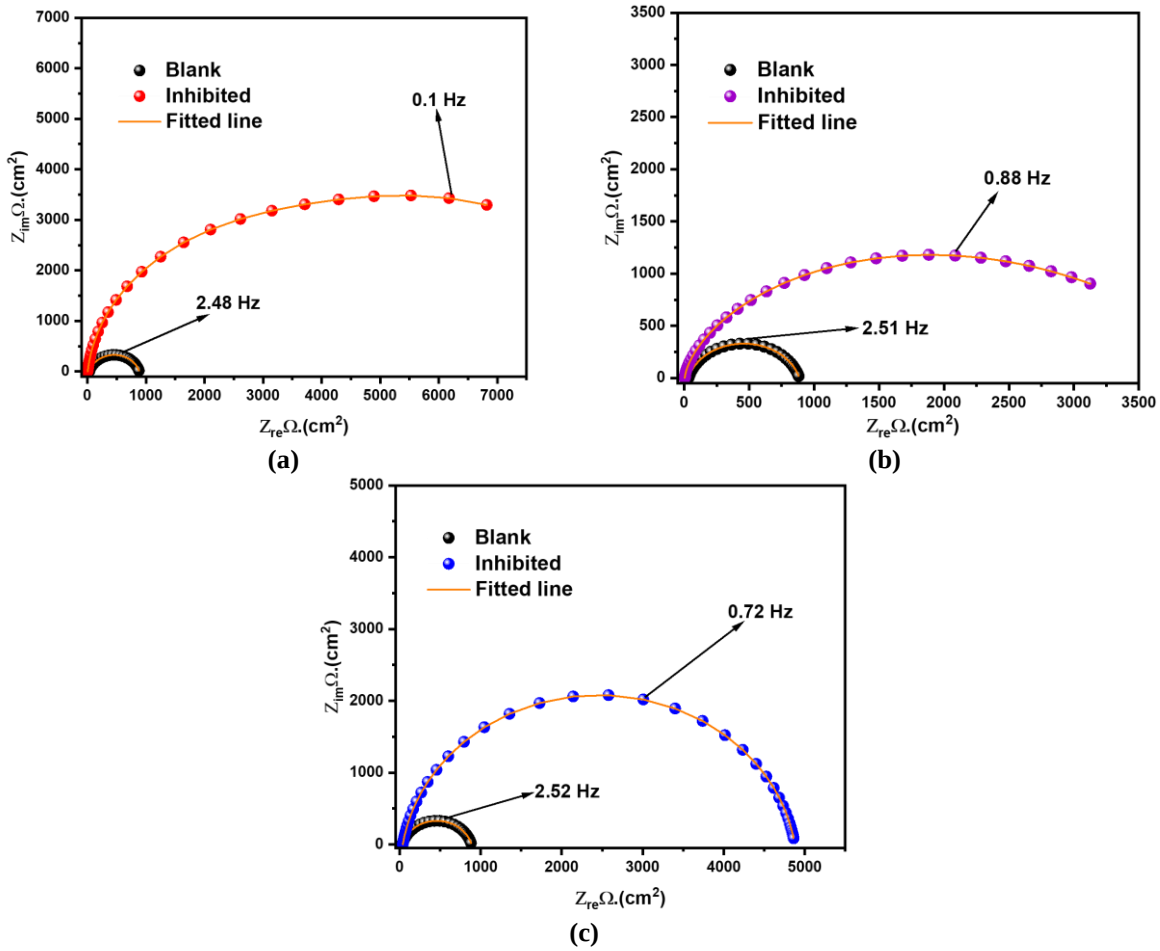

Figure 3. EIS plot of stainless steel for blank uninhibited system in comparison with the inhibited, tested in **(a)** 2H:1S solution; **(b)** S solution; **(c)** SH solution.

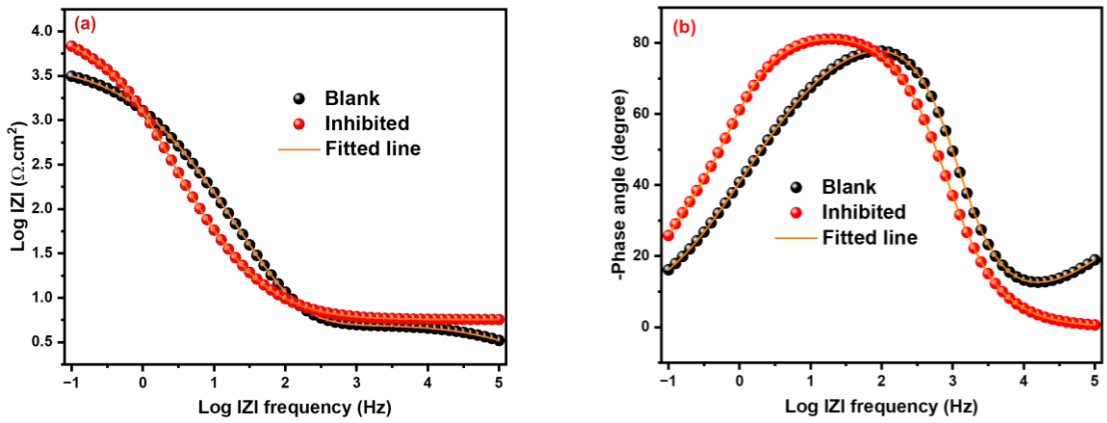

Figure 4. Bode plots **(a)** modulus; **(b)** phase angle for electrochemical impedance spectroscopy (EIS) analysis of stainless steel for blank uninhibited system in comparison with the inhibited, tested in 2H:1S solution.

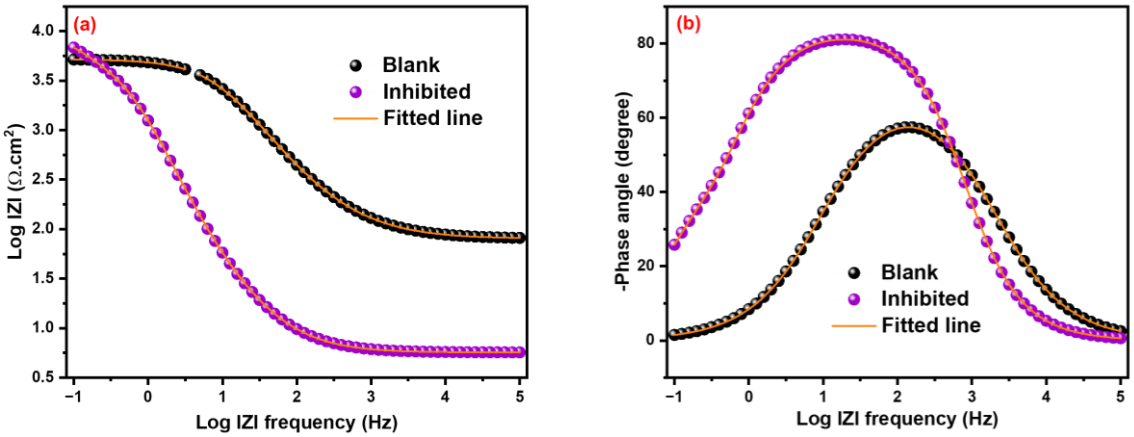

Figure 5. Bode plots (a) modulus; (b) phase angle for electrochemical impedance spectroscopy (EIS) analysis of stainless steel for blank uninhibited system in comparison with the inhibited, tested in S solution.

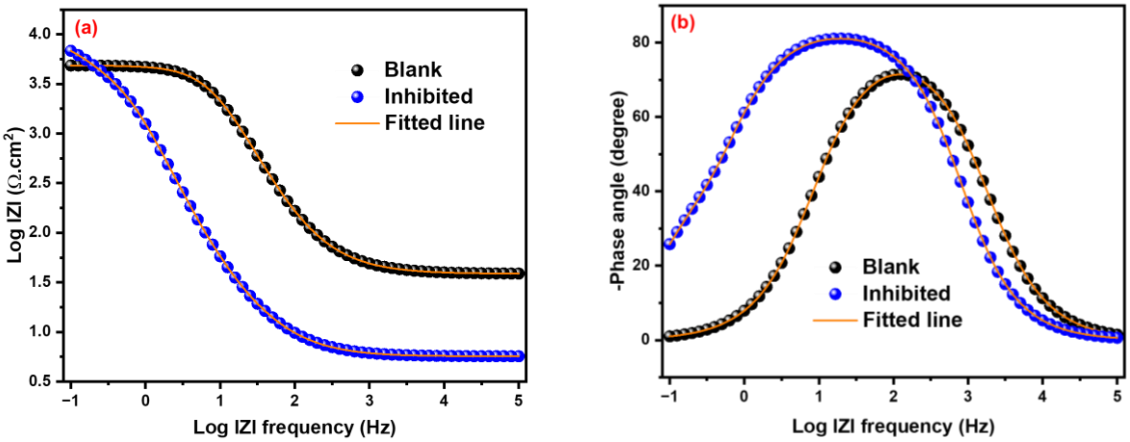

Figure 6. Bode plots **(a)** modulus; **(b)** phase angle for electrochemical impedance spectroscopy (EIS) analysis of stainless steel for a blank uninhibited system in comparison with the inhibited, tested in SH solution.

The corroborating evidence is further illustrated by the Bode plots, which show an increase in the impedance modulus and a shift toward more negative phase angles in the inhibited systems. This behavior indicates an enhancement in capacitive characteristics, likely due to the establishment of a uniform inhibitor layer. Elevated impedance values observed at low and medium frequencies in EIS for a corrosion inhibitor suggest the provision of effective corrosion protection [15,31]. These elevated values are associated with the development of a

stable and protective film on the metal surface, which substantially enhances the resistance against corrosive agents [15].

Comparative analysis of the three corrosive environments indicates that the inhibitor demonstrated optimal performance in the 2H:1S solution, achieving an inhibition efficiency (IE) that exceeds 93%. The lower efficiencies recorded in the S and SH solutions (82–85%) may be attributed to the impact of different ionic species present in the medium, which could influence the adsorption and film stability of the inhibitor molecules. However, all systems exhibited significant protection, confirming the broad applicability of the inhibitor in various environments.

Table 2. EIS data relating to stainless steel for a blank uninhibited system in comparison with the inhibited, tested in diverse media.

	System	R_s / Ω cm^2	R_{po} / Ω cm^2	Q1x10^{-5} / μΩ^{-1} s^n cm^{-2}	n1	R_{ct} / Ω cm^2	Q2x10^{-5} / μΩ^{-1} s^n cm^{-2}	n1	θ	IE/ %
2H:1S	Blank	18.12	80	110.5	0.86	708.40	14.27	0.88	-	-
	Inhibited	19.17	900.0	97.0	0.89	11070.0	9.41	0.98	0.936	93.6
Saline	Blank	18.19	80.0	111.4	0.88	707.90	17.00	0.87	-	-
	Inhibited	19.12	400.0	89.0	0.89	4100	13.10	0.89	0.827	82.7
SH	Blank	18.82	80.0	97.8	0.89	708.20	16.82	0.88	-	-
	Inhibited	19.04	500.0	89.0	0.94	4500	12.77	0.98	0.843	84.3

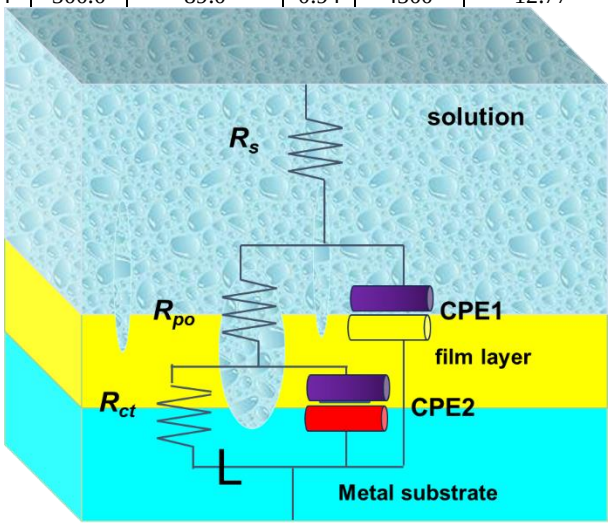

Figure 7. Electrochemical equivalent circuit fit for a stainless steel blank uninhibited system and an inhibited system at room temperature.

3.4. DFT analysis in gas phase.

3.4.1. Frontier molecular orbital (FMO) analysis.

The energies associated with the highest occupied molecular orbital (HOMO) and the lowest unoccupied molecular orbital (LUMO) are essential for understanding a molecule's capacity for electron donation and acceptance [39]. Figure 8 illustrates the optimized structure of mefenamic acid, including its HOMO and LUMO, as well as the electrostatic potential map. Table 3 presents the quantum chemical descriptors of mefenamic acid determined in the gas phase. An elevated HOMO energy suggests a strong ability to donate electrons to metal orbitals, which facilitates chemisorption [39, 40]. In contrast, a reduced LUMO energy indicates the molecule's effectiveness in accepting electrons from the metal surface, which permits back-donation.

In the case of MA, the HOMO energy value of -6.03 eV suggests a moderate capacity for electron donation, while the LUMO energy of -1.27 eV indicates a favorable ability to

accept electrons. This concomitant behavior promotes donor-acceptor interactions between the inhibitor and the metal surface [41]. The energy difference between the HOMO and LUMO, known as the HOMO-LUMO gap, serves as a critical indicator of stability [41]. A reduced energy gap in the inhibitor molecule is associated with enhanced inhibition efficiency, as it indicates a lower energy threshold for removing an electron from the lowest-occupied orbital [40]. The calculated energy gap (ΔE = 4.76 eV) implies that the compound maintains a level of chemical stability while being moderately reactive, thus favoring mixed adsorption mechanisms comprising both physisorption and chemisorption.

Table 3. Parameters obtained from DFT studies in the gas phase.

Compound	Mefenamic acid
Energy (au)	-785.85
E_{LUMO} (eV)	-1.27
E_{HOMO} (eV)	-6.03
Dipole (Debye)	6.37
Polarizability	61.16
I (eV)	6.03
A (eV)	1.27
Energy gap (eV)	4.76
χ (eV)	3.65
η (eV)	2.38
σ (eV^{-1})	0.42
ω (eV)	2.80
ΔN (eV)	0.70

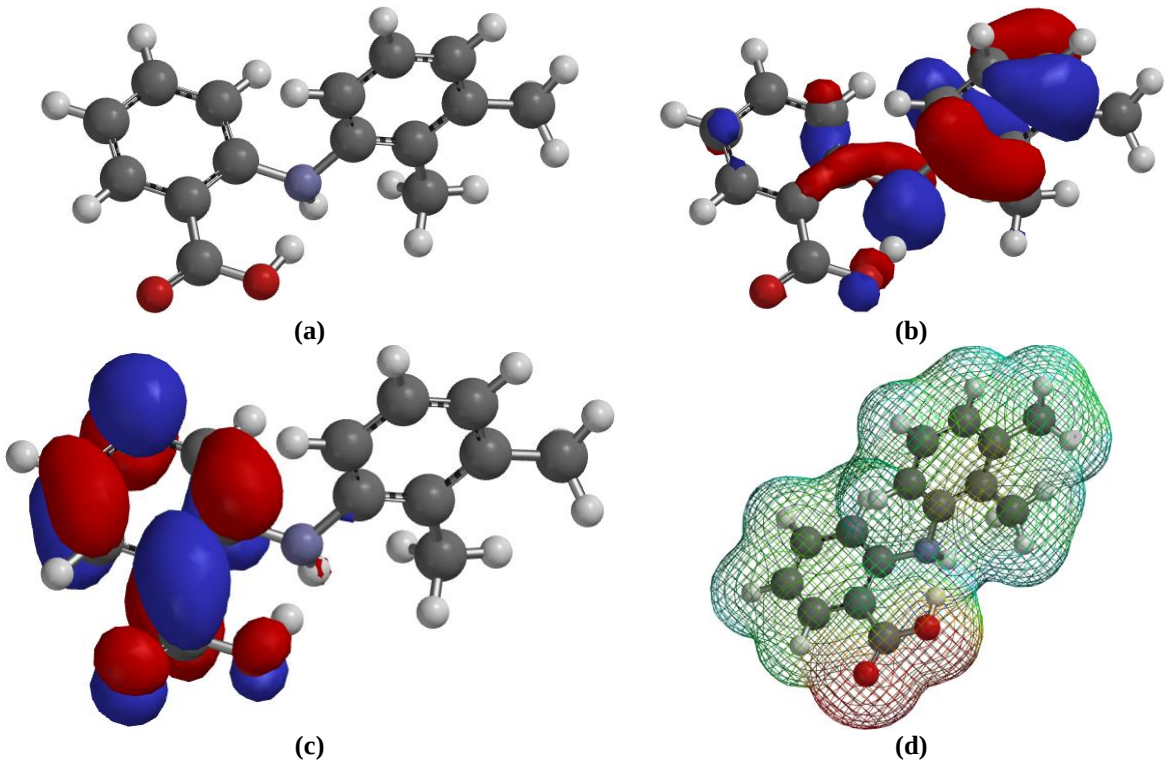

Figure 8. (a) Optimized structure of Mefenamic acid; **(b)** Mefenamic acid HOMO; **(c)** Mefenamic acid LUMO; **(d)** Electrostatic Potential Map in gas phase.

3.4.2. Electronegativity, hardness, softness, and electrophilicity.

Global reactivity parameters such as electronegativity, hardness, softness, and electrophilicity characterize the overall chemical behavior of the molecule [42]. The electronegativity value (χ = 3.65 eV) indicates that the molecule possesses a notable capacity for electron attraction, facilitating balanced donor–acceptor interactions with metal substrates.

Molecules with low global hardness or high global softness tend to be more reactive and are therefore better corrosion inhibitors. The values of η and σ obtained in this study are in agreement with those reported for a good corrosion inhibitor by Ouakki *et al*. [41]. The hardness (η = 2.38 eV) reflects resistance to charge transfer, signifying an equilibrium between the compound's stability and reactivity, while the value of softness (σ = 0.42 eV^{-1}) suggests a reasonable capacity for electron sharing, thereby enhancing effective adsorption on metal surfaces. Electrophilicity Index (ω = 2.8 eV): This suggests that the molecule exhibits a moderate ability to accept electrons, which aids in the back-donation process from the metal surface.

3.4.3. Dipole moment, polarizability, and charge transfer.

A dipole moment of 6.37 Debye suggests that the compound is significantly polar, allowing for robust electrostatic interactions between the molecule and the charged metal surface. The observed polarity contributes to enhanced molecular alignment and coverage on the metal surface, thereby reinforcing the protective film [41]. The polarizability value of 61.16 indicates the molecule's capacity to distort its electron cloud when subjected to an electric field, thereby amplifying van der Waals forces and dispersion interactions that are conducive to physisorption and the stability of the film. A positive value of ΔN suggests that electron donation occurs from the inhibitor to the metal, thereby validating the occurrence of donor–acceptor interactions [41]. The measured charge-transfer value indicates substantial adsorption strength and stability of the inhibitor layer.

3.4.4. Electrostatic potential.

Regions with a positive electrostatic potential indicate low electron density and a positive charge, whereas regions with a negative electrostatic potential indicate higher electron density and a negative charge. Electrostatic potential is frequently utilized to examine and predict various molecular properties, including reactivity and intermolecular interactions. In Figure 8d, the electrostatic potential map demonstrates that the O atoms in mefenamic acid exhibit increased electron density, which implies their capacity to engage with other functional groups in the formation of a complex, as evidenced by the red coloration in the corresponding region of the electrostatic potential map [42].

3.5. Quantum chemical descriptors determined in vacuum and water.

The chemical descriptors determined in vacuum and water are presented in Table 4, while the optimized structure, frontier orbitals, and electrostatic potential are presented in Figure 9. The overall electronic energy of the compound experiences a marginal rise from 786.08 au in a vacuum to 786.09 au in an aqueous environment. The energy of the highest occupied molecular orbital (HOMO) decreases from –5.66 eV in vacuum to –5.78 eV in water, indicating a greater stabilization of the HOMO within the aqueous phase. Correspondingly, the energy of the lowest unoccupied molecular orbital (LUMO) becomes more negative in water (–1.77 eV) compared to vacuum (–1.63 eV), suggesting an increased capacity for the molecule to accept electrons in a polar medium. The ionization potential (IP) rises from 5.66 eV in vacuum to 5.78 eV in water, aligning with the observed decrease in EHOMO. Similarly, the electron affinity (EA) grows from 1.63 eV to 1.77 eV when in water, indicating that the molecule is more inclined to accept electrons while solvated. The energy gap between HOMO

and LUMO decreases slightly from 4.03 eV in a vacuum to 4.01 eV in water. Generally, a smaller energy gap is associated with greater chemical reactivity and increased polarizability, as it requires less energy to excite electrons [43,44]. While the observed change is modest, it suggests that the compound may exhibit a modest increase in reactivity in aqueous environments [45]. The rise in χ in water signifies an amplified electron-withdrawing attribute, which is facilitated by the solvent's stabilization of negative charge density [43]. The electrophilicity index (ω) experiences an elevation from 3.30 eV in a vacuum to 3.55 eV in aqueous conditions. This increased ω value in water corroborates the compound's tendency to act as a more potent electrophile in aqueous media, thereby increasing its vulnerability to nucleophilic attack.

A comparative assessment indicates that aqueous solvation contributes to the stabilization of both occupied and unoccupied molecular orbitals, while also elevating the ionization potential, electron affinity, electronegativity, and electrophilicity. In addition, there is a slight reduction in the HOMO–LUMO gap. Collectively, these trends imply that MA is likely to exhibit greater electronic stabilization and heightened electrophilic character in water, leading to a subtly enhanced reactivity toward nucleophiles, all the while maintaining similar global hardness and softness.

Table 4. Chemical descriptors for mefenamic acid in vacuum and water.

Descriptor	Vacuum	Water
Energy (au)	-786.08	-786.09
E_{LUMO} (eV)	-1.63	-1.77
E_{HOMO} (eV)	-5.66	-5.78
I (eV)	5.66	5.78
A (eV)	1.63	1.77
Energy gap (eV)	4.03	4.01
χ (eV)	3.65	3.78
η (eV)	2.02	2.01
σ (eV^{-1})	0.50	0.50
ω (eV)	3.30	3.55
ΔN (eV)	0.83	0.80

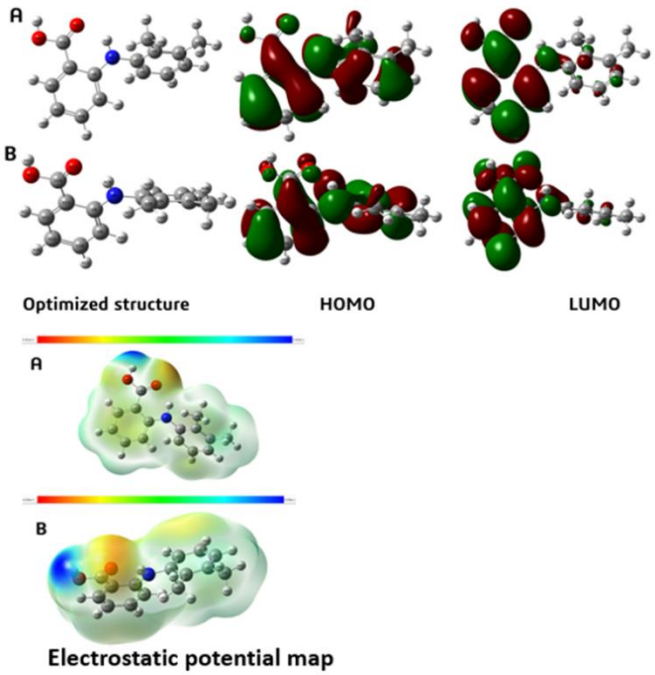

Figure 9. Optimized structure, frontier molecular orbitals, and electrostatic potential of MA in **(A)** vacuum; **(B)** water.

4. Conclusions

Electrochemical methodologies were employed to investigate the impact of mefenamic acid on the electrochemical properties of stainless steel 316 when exposed to three distinct environments: a 2:1 mixture of hydrogen peroxide and NaCl solution, NaCl solution alone, and a 50:50 mixture of NaCl and H_2O_2. The corrosion potential results demonstrated that mefenamic acid acted as a mixed-type inhibitor, successfully reducing both anodic and cathodic processes. A significant drop in corrosion current density was observed, along with a considerable upsurge in charge transfer resistance when the inhibitor was applied across all evaluated solutions. The highest recorded inhibition efficiency, at 93.6%, occurred with the use of 0.5 g/L of mefenamic in the 2H:1S solution. Density functional theory findings indicated that mefenamic acid possesses favorable characteristics that may enhance its performance as a corrosion inhibitor.

Future research might involve employing surface-sensitive techniques to thoroughly investigate the interaction mechanisms between the inhibitor and the steel substrate. Exploring the optimal inhibitor concentration to improve inhibition efficiency is also important for future research.

Author Contributions

Conceptualization, M.M.; methodology, E.K.; project administration, M.M., E.K., and N.O.; writing—original draft preparation, M.M.; writing—review and editing, M.M. and N.O.; formal analysis, M.M.; supervision, M.M.; visualization, M.M. and N.O.; data curation, M.M. and N.O.; investigation, E.K. and M.M. All authors have read and agreed to the published version of the manuscript.

Institutional Review Board Statement

Not applicable.

Informed Consent Statement

Not applicable.

Data Availability Statement

Data supporting the findings of this study are available upon reasonable request from the corresponding author.

Funding

This research received no external funding.

Acknowledgments

The technical assistance of Dr. V. I. Chukwuike of Federal University of Health Science, Uburu, Ebonyi State, is acknowledged.

Conflicts of Interest

The authors declare no conflict of interest.

Role of Funders

The funders had no role in the design of the study, in the collection, analysis, or interpretation of data, in the writing of the manuscript, or in the decision to publish the results.

Abbreviations

The following abbreviations are used in this manuscript:

Abbreviation	Definition
2H:1S	2:1 Mixture of Hydrogen Peroxide and Normal Saline
EIS	Electrochemical Impedance Spectroscopy
E_{corr}	Corrosion Potential
H_2O_2	Hydrogen Peroxide
I_{corr}	Current Density
IE	Inhibition Efficiency
MA	Mefenamic Acid
OCP	Open Circuit Potential
PDP	Potentiodynamic Polarization
S	Saline

References

1. Sultana, N.; Nishina, Y.; Nizami, M.Z.I. Surface Modifications of Medical Grade Stainless Steel. *Coatings* **2024**, *14*, 248, https://doi.org/10.3390/coatings14030248.
2. Eliaz, N. Corrosion of Metallic Biomaterials: A Review. *Materials* **2019**, *12*, 407, https://doi.org/10.3390/ma12030407.
3. Boraei, N.F.E.; Ibrahim, M.A.M.; Rehim, S.S.A.E.; Elshamy, I.H. Electrochemical corrosion behavior of β-Ti alloy in a physiological saline solution and the impact of H_2O_2 and albumin. *J. Solid State Electrochem.* **2024**, *28*, 2243-2256, https://doi.org/10.1007/s10008-023-05751-z.
4. Seethammaraju, S.; Rangarajan, M. Corrosion of stainless steels in acidic, neutral and alkaline saline media: Electrochemical and microscopic analysis. *IOP Conf. Ser.: Mater. Sci. Eng.* **2019**, *577*, 012188, https://doi.org/10.1088/1757-899X/577/1/012188.
5. Reclaru, L.; Grecu, A.F.; Grecu, D.F.; Lungulescu, C.V.; Grecu, D.C. Corrosion and Ion Release in 304L Stainless Steel Biomedical Stylets. *Materials* **2025**, *18*, 3769, https://doi.org/10.3390/ma18163769.
6. Maji, K.; Lavanya, M. Microbiologically Influenced Corrosion in Stainless Steel by Pseudomonas aeruginosa: An Overview. *J. Bio- Tribo-Corros.* **2024**, *10*, 16, https://doi.org/10.1007/s40735-024-00820-w.
7. Abbas, A.; Adesina, A.Y.; Suleiman, R.K. Influence of Organic Acids and Related Organic Compounds on Corrosion Behavior of Stainless Steel—A Critical Review. *Metals* **2023**, *13*, 1479, https://doi.org/10.3390/met13081479.
8. Zaffora, A.; Di Franco, F.; Santamaria, M. Corrosion of stainless steel in food and pharmaceutical industry. *Curr. Opin. Electrochem.* **2021**, *29*, 100760, https://doi.org/10.1016/j.coelec.2021.100760.
9. Makjan, S.; Boonsri, P.; Channuie, J.; Kanjana, K. Effects of hydrogen peroxide on 304 stainless steel in high temperature water. *J. Phys.: Conf. Ser.* **2019**, *1380*, 012087, https://doi.org/10.1088/1742-6596/1380/1/012087.
10. Gupta, M.; Chaudhary, M.Y.; Azad, N.; Yadav, S. Quantitative and qualitative insights into the corrosion mitigation mechanism of N, N-dibutyl aniline for mild steel in sulfuric acid. *Extreme Mater.* **2025**, *1*, 44-60, http://doi.org/10.1016/j.exm.2025.07.001.
11. Xu, Y.; Li, Y.; Chen, T.; Dong, C.; Zhang, K.; Bao, X. A short review of medical-grade stainless steel: Corrosion resistance and novel techniques. *J. Mater. Res. Technol.* **2024**, *29*, 2788-2798, https://doi.org/10.1016/j.jmrt.2024.01.240.
12. Sabiha, M.; Kerroum, Y.; El Hawary, M.; Boudalia, M.; Bellaouchou, A.; Hammani, O.; Amin, H.M.A. Investigating the Adsorption and Corrosion Protection Efficacy and Mechanism of *Marjoram* Extract on Mild Steel in HCl Medium. *Molecules* **2025**, *30*, 272, https://doi.org/10.3390/molecules30020272.
13. Xu, W.; Yu, F.; Yang, L.; Zhang, B.; Hou, B.; Li, Y. Accelerated corrosion of 316L stainless steel in simulated body fluids in the presence of H_2O_2 and albumin. *Mater. Sci. Eng. C* **2018**, *92*, 11-19, https://doi.org/10.1016/j.msec.2018.06.023.

14. Jessop, Z.M.; García-Gareta, E.; Zhang, Y.; Jovic, T.H.; Badiei, N.; Sharma, V.; Whitaker, I.S.; Kang, N. Role of hydrogen peroxide in intra-operative wound preparation based on an in vitro fibrin clot degradation model. *JPRAS Open* **2021**, *29*, 113-122, https://doi.org/10.1016/j.jpra.2021.04.008.
15. Simionescu, N.; Benea, L.; Chiriac, A. The Effect of H_2O_2 and Lactic Acid Addition in Biological Saliva on the Corrosion Behaviour of 304L Stainless Steel. *IOP Conf. Ser.: Mater. Sci. Eng.* **2020**, *877*, 012039, https://doi.org/10.1088/1757-899X/877/1/012039.
16. Sharma, A.; Kumar, V. Behavior of Steels against Corrosion in Peroxide Solutions. *J. Mater. Environ. Sci.* **2011**, *3*, 76-84.
17. Singh, A.K.; Chaudhary, V.; Sharma, A. Electrochemical Studies of Stainless Steel Corrosion in Peroxide Solutions. *Port. Electrochim. Acta* **2012**, *30*, 99-109, https://doi.org/10.4152/pea.201202099.
18. Ubaldini, A.; Telloli, C.; Rizzo, A.; Gessi, A.; Marghella, G.; Bruni, S.; Calistri, S.; Gennerini, F.; Pintilei, G. A Study of Accelerated Corrosion of Stainless Steels under Highly Oxidizing Conditions. *Coatings* **2024**, *14*, 390, https://doi.org/10.3390/coatings14040390.
19. Veysi, A.; Roushani, M.; Najafi, H. Synthesis and evaluation of CuNi-MOF as a corrosion inhibitor of AISI 304 and 316 stainless steel in 1N HCl solution. *Heliyon* **2025**, *11*, e41296, https://doi.org/10.1016/j.heliyon.2024.e41296.
20. Krasnodębska-Ostręga, B.; Drwal, K.; Sadowska, M.; Bluszcz, D.; Miecznikowski, K. Corrosion process of stainless steel in natural brine as a source of chromium and iron – the need for routine analysis. *RSC Adv.* **2023**, *13*, 28834-28842, https://doi.org/10.1039/d3ra04801b.
21. Gudić, S.; Nagode, A.; Šimić, K.; Vrsalović, L.; Jozić, S. Corrosion Behavior of Different Types of Stainless Steel in PBS Solution. *Sustainability* **2022**, *14*, 8935, https://doi.org/10.3390/su14148935.
22. Abdelfatah, A.; Raslan, A.M.; Mohamed, L.Z. Corrosion Characteristics of 304 Stainless Steel in Sodium Chloride and Sulfuric Acid Solutions. *Int. J. Electrochem. Sci.* **2022**, *17*, 220417, https://doi.org/10.20964/2022.04.29.
23. Chaouiki, A.; Chafiq, M.; Lgaz, H.; Al-Hadeethi, M.R.; Ali, I.H.; Masroor, S.; Chung, I.-M. Green Corrosion Inhibition of Mild Steel by Hydrazone Derivatives in 1.0 M HCl. *Coatings* **2020**, *10*, 640, https://doi.org/10.3390/coatings10070640.
24. Lgaz, H.; Chung, I.-M.; Albayati, M.R.; Chaouiki, A.; Salghi, R.; Mohamed, S.K. Improved corrosion resistance of mild steel in acidic solution by hydrazone derivatives: An experimental and computational study. *Arab. J. Chem.* **2020**, *13*, 2934–2954, https://doi.org/10.1016/j.arabjc.2018.08.004.
25. Hisyam, B.A.B.; Zain, Z.M.; Rasol, N.E.; Tajuddin, A.M. INHIBITION EFFECTS OF TRIDENTATE HYDRAZONE LIGANDS AS CORROSION INHIBITORS ON MILD STEEL IN SATURATED CO_2 ENVIRONMENT. *Malays. J. Anal. Sci.* **2024**, *28*, 220-235.
26. Odozi, N.W.; Saheed, R.; Mchihi, M.M. Application of *Peperomia Pellucida* Leaves Extract as a Green Corrosion Inhibitor for Mild Steel in 1.0 M Hydrochloric Acid Solution. *Chemsearch J.* **2019**, 10, 88–93.
27. Odozi, N.W.; Adetoba, A.S.; Mchihi, M.M.; Akpaetok, A.N. *Synsepalum dulcificum* Leaves Extract as Green Inhibitor for Mild Steel Corrosion in Hydrochloric Acid. *ChemSearch J.* **2021**, *12*, 47–54.
28. Mchihi, M.M.; Odozi, N.W.; Odimuko, A.B. Deciphering properties of *Dryopteris marginalis* as green corrosion inhibitor for mild steel in HCl: Electrochemical, gas chromatography and DFT studies. *Sustain. Chem. One World* **2025**, *7*, 100103, https://doi.org/10.1016/j.scowo.2025.100103.
29. Chioma, F.; Nnenna W, O.; M. Moses, M.; M. Abimbola, O. Synthesis, spectroscopic, and density functional theory studies of the corrosion inhibitive behaviour of n-(1,4-dihydro-1,4-dioxonaphthalene-3-yl)pyrazine-2-carboxamide chelator-ligand. *Glob. J. Pure Appl. Sci.* **2022**, *28*, 39-50, https://dx.doi.org/10.4314/gjpas.v28i1.6.
30. Odozi, N.W.; Emesiani, M.C.; Charles, C.D.; Seriki, B.O.; Mchihi, M.M. Electrochemical studies of the corrosion inhibitory potential of *Annona muricata* leaves extract on aluminum in hydrochloric acid medium. *FUDMA J. Sci.* **2024**, *8*, 395 - 401, https://doi.org/10.33003/fjs-2024-0803-2460.
31. Mchihi, M.M.; Olatunde, A.M.; Odozi, N.W. Ficus sur mediated synthesis of mesoporous ZnO nanoparticles and novel ZnO/Arginine/Tyrosine nanocomposite as eco-friendly corrosion inhibitors for mild steel in hydrochloric acid medium. *Mor. J. Chem.* **2024**, *12*, 1122-1152, https://doi.org/10.48317/IMIST.PRSM/morjchem-v12i3.42782.
32. Emesiani, M.C.; Umegbolu, V.C.; Mchihi, M.M. Corrosion inhibitory attributes of mixture of Codiaeum variegatum AND *Ficus benjamina* for mild steel in hydrochloric acid medium. *FUDMA J. Sci.* **2024**, *8*, 258-263.

33. Mchihi, M.M.; Odozi, N.W.; Gbolahan, S.A. Electrochemical Investigation of The Inhibitory Effect of Zinc Oxide Nanoparticles/Tenofovir Disoproxil Fumarate Nanocomposite on Mild Steel Corrosion in 1 M Hydrochloric Acid. *Anal. Bioanal. Electrochem.* **2024**, *16*, 559-567, https://doi.org/10.22034/abec.2024.714079.
34. Mchihi, M.M.; Emesiani, M.C.; Babawumi, J.I. Inhibitory Potentials of Leaf Extract of Justicia schimperi for Mild Steel Corrosion in Hydrochloric Acid Medium: Gravimetric, Microscopic and Spectroscopic Studies. *Asian Res. J. Curr. Sci.* **2023**, *5*, 184-192.
35. Mabrouk, D.H.; El-Morsy, F.E.; Alsam, A.A. Electrochemical studies, adsorption behavior, and spectroscopic analysis of vanadyl complex of bis(1-(pyridin-2-yl)ethylidene)malonohydrazide as efficient eco-friendly corrosion inhibitor for low carbon steel in 1M HCl. *Int. J. Electrochem. Sci.* **2024**, *19*, 100528, https://doi.org/10.1016/j.ijoes.2024.100528.
36. El-Aziz S. Fouda, A.; Al-bonayan, A.M.; Eissa, M.; Eid, D.M. Electrochemical and quantum chemical studies on the corrosion inhibition of 1037 carbon steel by different types of surfactants. *RSC Adv.* **2022**, *12*, 3253-3273, https://doi.org/10.1039/D1RA07983B.
37. Mchihi, M.M.; Olatunde, A.M.; Odozi, N.W. Electrochemical and Gravimetric Studies of the Corrosion Inhibitory Properties of Green Synthesized Copper Oxide Nanoparticles Mediated by Ficus sur for Mild Steel in HCl. *Jordan J. Chem.* **2025**, *20*, 81-93, https://doi.org/10.47014/20.2.1.
38. Mchihi, M.M.; Olatunde, A.M.; Odozi, N.W. CuO-based nanocomposite: synthesis, characterization, and evaluation of the corrosion inhibition effectiveness for mild steel in HCl: Original scientific paper. *J. Electrochem. Sci. Eng.* **2025**, *15*, 2715, https://doi.org/10.5599/jese.2715.
39. Malinowski, S.; Wróbel, M.; Woszuk, A. Quantum Chemical Analysis of the Corrosion Inhibition Potential by Aliphatic Amines. *Materials* **2021**, *14*, 6197, https://doi.org/10.3390/ma14206197.
40. Mchihi, M.M.; Odozi, N.W.; Nurudeen, A.O.; Emesiani, M.C.; Seriki, B.O. Assessment of Helianthus tuberosus leaves extract as eco-friendly corrosion inhibitor for Aluminum in sodium hydroxide: Insights from electrochemical, gravimetry and computational consideration. *Mor. J. Chem.* **2024**, *12*, 1462-1483, https://doi.org/10.48317/IMIST.PRSM/morjchem-v12i4.49160.
41. Ouakki, M.; Galai, M.; Rbaa, M.; Abousalem, A.S.; Lakhrissi, B.; Rifi, E.H.; Cherkaoui, M. Quantum chemical and experimental evaluation of the inhibitory action of two imidazole derivatives on mild steel corrosion in sulphuric acid medium. *Heliyon* **2019**, *5*, e02759, https://doi.org/10.1016/j.heliyon.2019.e02759.
42. El-Haitout, B.; Sardjono, R.E.; Es-Sounni, B.; Chafiq, M.; Salghi, R.; Bakhouch, M.; Al-Moubaraki, A.H.; Al-Ahmari, J.M.; Al-Ghamdi, A.A.; Fahim, M.; Hammouti, B.; Chaouiki, A.; Ko, Y.G. Electrochemical and quantum chemical investigation on the adsorption behavior of a schiff base and its metal complex for corrosion protection of mild steel in 15 wt% HCl solution. *Heliyon* **2024**, *10*, e40662, https://doi.org/10.1016/j.heliyon.2024.e40662.
43. Wahba, A.M.; Shoueir, K.; Fouda, A.E.-A.S. Prediction and evaluation of pyrimidinones derivatives: DFT analysis, corrosion inhibition, and bioactivity studies. *Results Surf. Interfaces* **2025**, *18*, 100448, https://doi.org/10.1016/j.rsurfi.2025.100448.
44. Shashirekha, K.; Aithal, S.; B.M, P.; M.K, P.; Guruprasad, A.M.; Devendra, B.K.; Rathod, M.R. Experimental, electrochemical and DFT simulation studies of a novel Schiff base derivative as an efficient mild steel corrosion inhibitor in acidic environments. *Results Surf. Interfaces* **2024**, *16*, 100246, https://doi.org/10.1016/j.rsurfi.2024.100246.
45. Numin, M.S.; Jumbri, K.; Kee, K.E.; Hassan, A.; Borhan, N.; Matmin, J. DFT Calculation and MD Simulation Studies on Gemini Surfactant Corrosion Inhibitor in Acetic Acid Media. *Polymers* **2023**, *15*, 2155, https://doi.org/10.3390/polym15092155.

Publisher's Note & Disclaimer

information before relying on it, and the publisher assumes no responsibility for any consequences arising from the use of materials contained in this publication.